T H E U N I V E R S I T Y O F M I C H I G A N

College of Engineering

Department of Nuclear Engineering

Laboratory for Fluid Flow and Heat Transport Phenomena

Report No. 07738-6-T
08466-1-T

HIGH SPEED PHOTOGRAPHIC STUDIES OF ULTRASONICALLY-INDUCED CAVITATION

H. G. Olson
F. G. Hammitt

Financial Support Provided by:
National Science Foundation
Grant No. GK-730

and

Army Research Office
Contract No. DAHC04 67 0007

July 1967

ABSTRACT

On the basis of photographic studies, it is indicated that the normal collapse mode for a bubble in an ultrasonically-induced cavitation field is asymmetrical. In most cases, the bubble involutes into a torus, the direction of the involution being dependent on perturbations of the bubble surface due to pressure gradients, etc. A vortex ring is formed producing a central microjet, the impact of which upon a solid surface is believed to be the predominant damaging mechanism. Three collapse models are hypothesized to explain the existence of the various types and sizes of cavitation bubbles which were observed, and to also suggest the mode of a possible damaging collapse. An attempt is made to correlate the known pit damage on an individual specimen to the approximate number of observed bubbles of the type that are believed to be indicative of such a jet impingement on the specimen surface, and it is found that the order of magnitude is correct. Visible evidence of the effect of the shock waves that apparently accompany rebounding bubbles is presented.

INTRODUCTION

It has been proposed in the past[1] that the vibratory horn system become the accepted standard for cavitation damage testing, and the possible adoption of this system is currently under study by the American Society for Testing Materials.* The cost for vibratory tests is considerably less than that for venturi or other flowing system tests both because of low initial cost and reduced testing time to achieve a desired degree of damage. However, the controlling parameters of the vibratory system differ so greatly from those of a flowing system that the vibratory data is difficult to apply. Hence, it is of paramount importance that all aspects of the vibratory damaging process and the resultant damage be thoroughly examined so that testing and rating of specimens will be meaningful. The study described in this paper attempts to provide some of the necessary information.

EXPERIMENTAL APPARATUS

The ultrasonic transducer unit used in this experiment (Fig. 1) was developed, constructed and originally used by Garcia.[2,3]

The remaining parts of the system include an audio-oscillator, a power amplifier, an oscilloscope, a frequency counter, an accelerometer,

---

* ASTM Committee G-2 on Cavitation and Impingement Erosion.

and a container for the water. The signal supplied by the variable frequency audio-oscillator is amplified and applied to the piezoelectric crystals. The standing waves that are generated in the axial direction are amplified by the exponential shape of the horn.

The metal specimens to be tested were selected from materials with widely differing mechanical properties in an attempt to correlate damage with specimen properties. This was another goal of the overall experiment. The specimens were metallographically polished before exposure. One specimen was lightly abraded with emery cloth and was used to examine, by photographic means, the effects of minor surface roughness on the bubble field population. Also, half the polished surface of one specimen was lightly abraded to test the effect of such a surface on the cavitation bubble field.

Because of the short duration of the acoustic cycle (range of 50 to 160 microseconds for these tests), and because of the extremely short formation and collapse times of the cavitation bubbles, it is mandatory that high-speed photography techniques be employed if meaningful visual information about the cavitation bubble cloud is to be obtained. While it would be desirable to use a camera with a capability of about 10^6 frames per second with a sufficient total number of frames to record such short duration events as the expansion and collapse of a bubble, equipment limitations prevented this.

A Beckman and Whitley Model 326 Dynafax camera was used throughout the experiment. This camera uses a rotating film drum and a rotating octagonal mirror to expose a maximum of 224 frames at a maximum framing rate of 26,000 frames per second. Utilization of "stops" permits a minimum exposure time per frame of about one microsecond at the maximum framing rate. At this framing rate, the time between corresponding points of successive frames in a sequence is 38.5 microseconds. A 1,000 joule light source with xenon flash tube was constructed and used. For the photographs showing the specimen surface, the vibrating horn was tilted so that its axis was approximately 30° from the horizontal. Using this procedure, depth of field limitations were lessened. The light blast was initiated beneath the water container and the light reflected from the specimen surface. Profile photographs were made with the horn held vertically and the light source positioned behind the specimen. The camera operates with an open shutter, so the duration of the light blast controlled the number of exposed frames. 35 mm Kodak Plus X or Tri X film was used. Development was done by the authors using Kodak or Acufine developers.

To study the reproducibility of cavitation bubble field patterns in a large number of successive frames, the oscillator frequency of the transducer system and the camera framing rate were matched as closely as possible using a Hewlett-Packard Dymec computing digital indicator.

This system was also used to increase the camera framing rate two per cent above that of the oscillator frequency, so that the entire acoustic cycle in a particular photographic run would be explored.

THEORY, ULTRASONICALLY-INDUCED CAVITATION BUBBLE FIELDS

The ultrasonic transducer provides high frequency mechanical vibrations at the end of the horn which generate an acoustic field in a fluid into which the horn is submerged. This can result in cavitation at the horn tip on the face that is normal to the direction of vibration. Cavitation for the present purpose is defined as the generation of and collapse of individual bubbles in an aggregate called the cavitation bubble field, the field occurring on and near the surface of the specimen. The forcing function for the generation and collapse of the bubbles is the time-varying pressure in the liquid that is adjacent to the specimen caused by the mechanical vibration of the horn tip. The bubbles presumably originate from some form of gas "nuclei" growing primarily during the negative pressure portion of the acoustic cycle and collapsing in a part of the positive pressure portion. Noltingk and Neppiras[4] computed this behavior, developing equations for the acoustically-induced motion of gas-filled bubbles. They assumed an incompressible liquid and neglected the vapor pressure in the bubble. They considered the mass of gas in the bubble to be constant and that

the applied acoustic wave was exactly sinusoidal. They then solved the equations numerically, and were able to predict the growth and collapse patterns for the bubbles under various acoustic conditions.

They showed that there is a size range of nuclei that will permit growth and collapse of the bubble in one acoustic cycle, completing the cavitation event as defined acoustically. Flynn[5] defines this type of bubble as the transient type.

If the bubble nucleus is of a proper size for the applied acoustic frequency, it will resonate with that frequency, pulsating under the action of the acoustic field in a series of complex oscillations, and fails to collapse in one cycle as the transient bubble does. Flynn's theoretical study[5] shows that resonant bubbles will oscillate under the action of the acoustic pressure with an amplitude that increases with time. If the diameter is increased sufficiently through miscellaneous perturbations, rectified diffusion, etc., it has been shown[5] that collapse of such a bubble is possible. This can be visualized from the view that the inward liquid inertial forces during contraction become sufficient to overcome the pressure buildup inside the bubble at a rate sufficient to allow completion of the collapse before the next negative acoustic pressure cycle becomes predominant.

Theoretically, a bubble collapse under the action of positive pressure starts slowly, but in the final stages, the bubble wall velocity for an empty cavity becomes very high. A collapsing bubble

containing gas and/or vapor collapses to some minimum diameter where the increased pressure of the contents (or centrifugal forces if the collapse results, as it sometimes appears, in a ring vortex) has balanced the collapsing pressure and liquid inertia, provided the bubble does not disintegrate during the collapse process because of surface instabilities. After the arresting process has been completed, the bubble can then conceivably either shatter into a few or many smaller bubbles, or rebound, appearing again as one large bubble. During rebound, the bubble or bubbles could disintegrate through some form of instability or expand in one or more acoustic cycles to a diameter where a cavitation collapse is again possible. During the original rebound, it is also possible for the bubble to reach this collapse diameter.

Thus, a cavitation bubble field around a vibrating horn consists of transient bubbles that grow and collapse in one acoustic cycle, and bubbles which apparently have rebounded from a collapse and exist for one or more additional acoustic cycles, their mean diameters being equal to or greater than the mean resonance diameter. The rebounding bubbles often grow immensely during one or two cycles after the rebound. Willard[6] mentioned a phase of the cavitation cycle where a large bubble vibrated with immensely increasing amplitude. He noted no final collapse.

The actual damaging mechanism from a collapsing bubble is still the subject of considerable conjecture. There is some evidence that cavitation damage in a flowing system[7,8,9,e.g.], is probably caused by the asymmetrical collapse of bubbles which evolve into a micro-jet which in turn impacts and damages the surface. The micro-jet theory[10,11] is opposed to the classical theory originated by Rayleigh[12] in his early analysis of the spherical collapse of a bubble in an ideal fluid, whereby it was postulated that a shock wave resulting from the collapse caused the damage.

Recent numerical calculations[13,14] using real fluid properties showed that the shock pressures generated by symmetrically collapsing bubbles were not sufficient to cause the observed damage, assuming no substantial motion of the collapse center, although this is a theoretical possibility, whereas the shock pressures from a symmetrically rebounding bubble could generate sufficient pressure to cause the damage within a distance equal to the bubble radius that existed when the collapse sequence began.

Cavitation damage in many cases suggests that it is initiated by single bubble collapses which produce single craters.[15] These craters are randomly dispersed over the surface, having little regard to grain boundaries, etc. Eventually, most of the exposed surface is damaged by

craters, so that gross fatigue failures then occur. Of course, it is also true that some individual blows are not of sufficient intensity to cause a crater in one event. Still their cumulative effect may be sufficient to cause eventual fatigue failure.

The profiles of individual pits show that they are approximately symmetrical and are surrounded by a small rim; however, a slight non-symmetry of the rim in flow-induced cavitation and the dependence of this non-symmetry on flow velocity, was taken as evidence for the existence of the jet rather than shock wave damage mechanism. Cavitation pits closely resemble pits obtained by impacting liquid[16] or metallic spheres on a test surface. Typical cavitation pits are shown in Fig. 2.

HIGH SPEED PHOTOGRAPHS OF THE CAVITATION BUBBLE FIELD

Figs. 3 and 8 are typical of the individual high speed photographs taken with an oscillator frequency of approximately 20,000 cps., camera framing rates of 20,150 and 26,000, and exposure times of 1.3 and 1.0 microseconds, respectively. Figs. 4 and 6 were photographed at 1.0 microsecond exposure with a camera framing rate of 26,000 with oscillator set at 10,000 cps. These photographs show transient bubbles typically from 0.003 to 0.020 cm. in diameter, bubbles at approximately the mean resonance diameter (0.032 cm. for 20,000 cps. and 0.064 for 10,000 cps.),

and also those bubbles that are greater than the respective mean resonance diameters and have apparently rebounded to this large size. The transient bubbles were only slightly larger at 10,000 cps. than at 20,000 cps. This is a result of the longer vibratory period combined with the reduced acoustic pressure. The latter is due to a reduced attainable horn amplitude at this frequency (the amplitude was approximately 0.038 mm. at 10,000 cps. and approximately 0.050 mm. at 20,000 cps.), and because the acoustic pressure varies directly as the frequency with other acoustic conditions remaining constant. The abrading of one half of the surface in Fig. 4 made no apparent difference in the relative bubbles population.

Extensive photographic studies were made of the cavitation bubble fields. It was noted that when the oscillator frequency and the camera framing rate were matched, the bubble pattern reproduced almost identically from frame to frame in the entire photographic run, but that small changes in the relative positions and groupings of the transient bubbles suggested that bubbles in this size range existed for only one acoustic cycle. Those bubbles at or larger than the mean resonance diameter could be readily identified from frame to frame by their size, shape and position. It was noted that these larger bubbles persisted over many frames, increasing continuously in size until they disappeared.

When using approximately matched oscillator frequency and camera framing rate as in Fig. 3, the selection of the point of the acoustic cycle which is examined is entirely random. Since the transient bubble population was observed in all but one of many such photographic sequences, it is concluded that they must be visible during a large part of the acoustic cycle. Because the bubble pattern was reproducible frame to frame in the individual photographic runs, with the exception of local, approximately circular clear areas around rebounding bubbles (to be discussed later), it is apparent that the technique applied of advancing the camera framing rate at a speed two per cent greater than the oscillator frequency permits a meaningful exploration of the entire acoustic cycle. Using this method it was established that at certain points in the acoustic cycle (which repeated cyclically) no transient bubbles existed, indicating that the positive acoustic pressure was then near its maximum.

Such exploration of the acoustic cycle gives experimental proof of Noltingk and Neppiras's[4] hypothesis that the transient bubbles make up the vast majority of the cavitation bubble field and grow and collapse in one acoustic cycle. Larger bubbles at or near the mean resonance diameter persist for more than one cycle.

By adjusting the oscillator frequency to 10,000 cps. and operating the camera at its maximum framing rate of 26,000, it was possible to obtain two or three photographs during the 100 microsecond duration of

each acoustic cycle. Fig. 4, six sequential photographs taken under these conditions shows the changes in the transient bubble population and the existence of the larger bubbles for more than one cycle. Fig. 4 (a) shows a fully-developed bubble star pattern that is a typical formation occurring at medium acoustic pressures. Bubbles in the transient size range are intermingled with larger ones, most of which are considerably larger than the predicted mean resonance diameter. In Fig. 4 (b), 38.5 microseconds later, practically all of the transient bubbles are gone, with the survivors being the same larger bubbles as can be seen by close examination. The diameters of these, however, are smaller than in (a). Assuming that (b) was photographed near the positive pressure peak, then knowing the interval between pictures, (c) must be at a position early in the negative portion of the cycle. This photograph should then show partial development of the transient bubble field and re-expansion of the larger bubbles. This interpretation is indeed consistent with the photograph. Fig. 4 (d) then must show the larger bubbles and the transient bubbles near their maximum diameters, as appears to be the case, since it would have been photographed somewhat after the minimum pressure point in the cycle, and bubble diameters would lag the pressure due to inertial effects. The larger bubbles of (d) can be readily matched by relative size and position with those in (c), as can some of the transient bubbles. Fig. 4 (e) shows the bubble field again

near the positive peak pressure part of the acoustic cycle, apparently after the collapse of the transient bubbles. Fig. 4 (f) again in the negative pressure portion, shows the larger bubbles, still easily identifiable because of their relative positions and a new group of transient bubbles.

A sinusoidal acoustic cycle and the probable approximate cycle positions which best match the photographic evidence regarding bubble population and the known frequency and framing rate are shown in Fig. 5. From this construction, one would deduce that Fig. 4 (a) and (f), and also Fig. 4 (b) and (e) should be similar, and they are. As stated previously, all the bubble fields shown are consistent with this interpretation of the timing sequence. The existence of transient bubbles and of larger bubbles which persist through more than one acoustic cycle, is thus verified.

The charcoal-like smudges which appear in Figs. 3 (a), (b), and (c) (some marked with arrows in Fig. 3 (b)) during the early growth of a transient bubble field are thought to be bubbles rebounding from a complete collapse as was described earlier. As a result of the rebounding, they have a roughened light-absorbing surface that cause this appearance. An alternative possibility is that the surface, or possibly the entire vaporous mass, may be composed of a myriad of very small diameter bubbles. Some of the bubbles that have apparently

rebounded to their full size are also extremely dark on the photographic prints. However, they show a spiny surface structure as shown in Figs. 15 (a) and (b), if sufficient filters are used during the printing process. A possible explanation of the great capability for light absorption of this type of bubble is afforded if it is assumed that these are actually clusters of bubbles. The spherical surfaces of the individual minute bubbles making up the cluster would act as lenses so that little light is reflected back to the camera. The ordinary smooth bubbles, though, are highly reflective and do return considerable light to the film. After a bubble has fully rebounded and oscillated in the acoustic field for one or more cycles, it recovers its original smooth, glossy appearance, but may have peculiar protuberances which we believe are the result of the rebound process (discussed later).

The existence of presumed rings of high-pressure liquid around many of the charcoal-like bubbles in the three photographs of the sequences of Fig. 3 can be seen. These "shock rings" may be similar to those observed by Schmid[17] in his single bubble experiments. Fig. 3 (a) shows a fairly heavily populated bubble field, apparently from some portion of the negative pressure part of the cycle, judging by the size of both the transient and the larger bubbles. Fig. 3 (b) shows a large number of bubbles with light-absorbing roughened surfaces that have apparently collapsed completely and are rebounding according to the arguments previously presented. Note the cleared area around

the rebounding bubble in the center of the specimen (marked by an oblique arrow). It is thought that the local high pressure region, presumably caused by the rebound, has collapsed the other bubbles in this circular area or else has prevented their growth from the nuclei. Since (a) and (b) are successive frames for conditions where the oscillator frequency and camera framing rates are almost matched, they show approximately the same part of the acoustic cycle. Thus the difference in population of the transient bubble field is significant. Fig. 3 (c), one cycle after (b), shows large, roughly circular cleared areas, and also a heavy bubble population in other areas. Some of the rebounding bubbles in (b) can be matched with those in (c) (the center one is marked with an oblique arrow of (c)), but their appearance is different. In (b) they were apparently rebounding after a collapse. In (c), judging by their size and glossy surface, it is thought that they have survived the previous positive pressure portion of the cycle without collapse. However, there are several new rebounding bubbles in (c) (marked by vertical arrows) which have apparently collapsed the small bubbles in their vicinity.

Additional photographic evidence of the effect of such shock rings can be seen by examining Figs. 6 (a) and (b), which are taken out of sequence from the same photographic run. Fig. 6 (a) shows the full star-like bubble cloud with some bubbles out of focus because of the

small depth of field of the camera lens system and Fig. 6 (b) shows a mist in the central area of the photograph which may be interpreted as smaller bubbles which are the debris from larger bubbles that were collapsed by the shock wave from the rebounding bubble at the center of the region. By reconstructing the sequence, (b) precedes (a) in the acoustic cycle by 7.5 microseconds. As will be pointed out later, the "bar-bell" bubbles seen in (a), (marked by vertical arrows) are believed to indicate that this photo was taken precisely at the bubble collapse point. The bubble field shown in (b) passed through the phase shown in (a), 7.5 microseconds previously and the large bubble in the center (marked with a vertical arrow) apparently has experienced a collapse and subsequent rebound in this period.

MODELS OF COLLAPSING BUBBLES AND A SUGGESTED DAMAGE MECHANISM

On the basis of photographs which are included and are typical of many hundreds that were examined, it is felt that the normal collapse mode for a cavitation bubble in the type of facility used for this experient is asymmetrical. Such asymmetry may be induced by the asymmetrical pressure distributions which would also control its directional dependence. As indicated also by studies in other systems,[7,15] the bubble may involute, forming a vortex ring or torus which may then produce a micro-jet which impacts the surface causing the observed damage.

Three models are suggested to describe bubble collapse, rebounds and a possible damage mechanism as shown by the present photographs. Fig. 7, Model A, describes the axially-symmetrical collapse and rebound of a spherical bubble. Portions of this model show similarities to sequences of high-speed photographs made by Ellis[18] where bubbles were formed in water at reduced pressure and collapsed by admitting air at atmospheric pressure to the water's surface. In Model A, through the action of the acoustic pressure field, the once spherical bubbles assume a bar-bell shape at the start of their collapse sequence. The ends of the bar-bell become unequal in volume with the difference in volume between the two ends increasing as the bubble collapses. The involution into a ring vortex apparently occurs near the peak of the positive pressure cycle since both the torus and the pinched-off section opposite the jet (formerly the small end of the bar-bell) are compressed to very small volumes. The energy for rebound can be stored in the vapor and/or gas in the "voids", in the elasticity in the water and/or in the centrifugal field of the torus which is presumably a closed-end ring vortex similar to a "smoke ring". The rebound of the torus, the pinched-off end, and the mass formed during the deceleration of the jet in the water completes the sequence. A collapse and rebound of this type where the jet was decelerated in the water before it could strike an adjacent surface would presumably cause no damage. The

irregular mass that appears at the point where the jet is arrested is apparently vapor resulting from the jet-induced local cavitation. The diverging shape of this mass suggests the form of a free jet in a quiescent fluid.

The peculiar and characteristic bar-bell shape of the bubble at the start of the collapse sequence just prior to the jet formation as in Model A-1, can be seen in many of the bubbles in Fig. 8. Their axes are uniformly perpendicular to the specimen surface. A typical bubble is marked with an arrow at the right of the photograph. The bar-bell bubbles marked on Fig. 6 (a) are similar to Model A-3. Another bubble resembling Model A-3 is indicated on Fig. 9, which is a profile photograph with the axis of the horn tilted slightly toward the camera thus showing a small portion of the specimen surface. No photographic indication of a jet at its minimum diameter, maximum velocity point as in Model A-4 was found in the hundreds of high-speed photographs that were studied (this phase of the bubble collapse exists for only a fraction of a microsecond, so the lack of a photographic image in a random-time-sampling method such as was used is not surprising), but the characteristic shapes of bubble sections after rebound as in A-5 were often observed. The best example of these is Fig. 10 which proves almost conclusively the existence of the toroidal type of collapse, although admittedly not its predominence.

The rebound could be consummated with the sections remaining intact or the sections could shatter. Figs. 11 (a) and (b) both were taken from a sequence where the oscillator frequency was set at 6,200 cps. and the horn amplitude was extremely small (because of a low intensity born resonance). The photographs were made at a framing rate of 26,000 and with an exposure time of one microsecond. On Fig. 11 (a) some of the bubble masses (marked with arrows) suggest rebounds into toroidal shapes. Others, as shown in the upper portion of the photograph, appear irregular and shattered. Fig. 11 (b) shows long narrow shapes. The one at the upper central part of the photograph (marked with an arrow) apparently casts a shadow.

The frothy regions often seen near the rebounded bubbles may be due to the vapor trail created by the high-velocity liquid jet passing through the torus. Fig. 12, a profile photograph, appears to show a rebounded "pinched off" section (marked with arrow) similar to one section of Model A-5 and many jets, the most prominent jet being at the narrow end of the "pinched off" section where it is directed toward the specimen surface.

A second model is conceived relative to the large hemispherical bubbles that have been observed by many experimenters[6,e.g.,] to be on the specimen surface. These seem to persist without collapsing. This model is also consistent with the collapse and rebound behavior

on a surface of spark-induced hemispherical bubbles.[11,19] In the present investigation, it had been noticed that such bubbles persist for 3 to 50 or more acoustic cycles, but eventually they disappear, probably after a final collapse. Fig. 7, Model B-1 shows such a hemisphere on the surface and B-2 shows a helmet-like shape (this shape is often noted in cavitating venturi tests during the collapse sequence[13]). In B-3 the bubble assums a more cylindrical shape with a small button on top. These first parts of the sequence are identical with those shown in high-speed photographs of spark-induced bubbles by Shutler and Mesler.[19] Apparently because of proximity to the surface or perhaps because the required collapse time is too long to be completed before the effect of the negative pressure portion of the cycle is felt, the jet does not develop sufficiently to complete the collapse through the torus, but as is shown in B-4, it apparently scatters back through the torus forming a large bubble that is seated on the rebounded torus (as in B-5). Instabilities during the rebound or collapse could probably cause the protuberances often observed on bubbles after an apparent rebound. These could also be caused by micro-jets generated by the bubble wall motion (as was previously discussed) which penetrate the bubble surface or are deflected from an adjacent solid boundary. Such jets could cause additional local secondary cavitation which could appear as strings of bubbles attached or adjacent to the rebounded bubble. The

"shaped charge" effect caused by accelerating concave liquid surfaces has been observed in many experiments[20,e.g., Engel[16] has concluded that for a liquid drop striking a hard surface with a subsonic liquid velocity, radial flow velocities up to eight times that of the impinging velocity could occur, since the pressure in the impact area approximates the "water hammer" pressure rather than the conventional stagnation pressure. Similar observations have been made in this laboratory. Thus, even for a relatively weak jet, the resultant scatted or deflected jets could obtain sufficiently high velocities to cause secondary cavitation.

The large bubble mass at the upper left and the one slightly below it (both marked by arrows) in Fig. 8 typify the rebounded mass as suggested by Model B-5. Note the symmetrical strings of bubbles around the upper bubble. The rebounded bubble mass sitting on the rebounded torus can be seen in both bubbles. These large bubbles have apparently resulted from a rebound during the negative pressure portion of a previous acoustic cycle since the bar-bell shaped transient bubble field indicates the start of a collapse sequence.

Fig. 13 (a), a profile photograph, shows a typical hemispherically-shaped bubble as shown in Model B-1. Fig. 13 (b), a photograph with the horn axis tilted slightly towards the camera, shows shapes similar to B-2. Figs. 14 (a) and (b), photographs with the horn axis tilted slightly toward the camera and a profile show, respectively, shapes similar to

Models B-3 and B-4. The various bubbles are indicated by arrows. Because of the relatively slow framing rate only hints could be obtained as to the correctness of the various model sequences.

A third model is suggested as shown in Fig. 7, Model C, to explain the rapid growth of newly rebounding bubbles, the bubble-free areas around these bubbles, and hopefully one of the actual damaging mechanisms. Model C-1 shows hemispherically-symmetrical scattering of a micro-jet from a bubble collapse, the micro-jet possibly evolving from the sequence shown in Model A. However, it is now assumed that the event occurs under circumstances ideal for producing damage. These circumstances involve jet energy, proximity to specimen surface, surface conditions, etc. (e.g., a previous pit may provide suitable jet guidance and amplification of the effect). These reflected jets, as mentioned previously, may possess velocities considerably in excess of the original impinging jet and could cause considerable localized secondary cavitation as they pass through the liquid. The collapse and rebound of the bubbles in the wake of these scattered jets could cause the localized over-pressure that is evident because of the absence of nearby bubbles. This over-pressure also could be caused by the rebound of the bubble as a whole. The high pressure region that apparently exists around the rebounding bubbles could then persist until all of the activity has ceased. The rebounding conglomeration probably includes the previously discussed torus and

pinched off section of the collapsing bubble, both of which could have been shattered by the reflected jets. The mass as in Model C-2 takes on a spiny appearance. As previously discussed, it reflects little light. In C-3, the bubble rebounds to full size, but the surface is very rough. In C-4, after fully rebounding or possibly after oscillating in the acoustic field, the bubble is smooth and lustrous as in B-1.

The damaging types of collapses are presumably those of initially spherical bubbles on or immediately adjacent to the specimen surface, and as a result of this study and other confirmatory evidence, it is felt that the predominant damaging mechanism in the vibratory horn cavitation regions is the micro-jet impact. Collapses consistent with the generation of such jets appear to be the predominant type observed in this study. The pressure pulses arising from collapse and rebound of the bubble sections remaining after the typical toroidal collapse seem likely to be too weak to cause the observed damage, although Shutler and Mesler[19] did observe damage in their tests on soft lead under the rebounding torus. The non-spherical bubble fragments remaining after a collapse are probably highly unstable and are observed in this experiment to disappear during the next positive pressure cycle.

Since the bar-bell bubble on the specimen surface is observed always with its major axis approximately normal to the surface (those which are slightly off of the surface have been noted to be at an angle from the

normal), those most energetic micro-jets that are directed to the surface should impinge approximately normally so that the resultant crater should have a symmetrical raised rim. Only symmetrical rims were found on all the pits from these vibratory tests for which the profiles were studied by a precision profilometer, although the rims are very small. This normal impingement of the micro-jets in the present study could also explain the consistent symmetry of those rapidly expanding rebounding bubbles that probably originate from a collapsing bubble as in Model C. The massive bubble formation as in C-3 can be seen in Figs. 15 (a) and (b) (bubbles are marked by horizontal arrows). The bubble indicated by the oblique arrow in Fig. 15 (b) is more massive than the other bubbles also shown, but is only partly visible because of filters used in the printing process.

Examination of the photographs indicates that there are from two to five rebound bubbles originating in each cycle. Estimating, for example, an average of 3.5 rebounds per cycle and a 30 second run at 20,000 cycles per second, the specimen would be exposed to 2×10^6 such collapses and rebounds. For such an exposure, less than 100,000 pits have been detected, even for one of the softest materials used, type 1100-0 aluminum. However, few rebounds are so massive as those shown in Figs. 15 (a) and (b). These occur roughly twice in an experimental run which usually includes a usable photographic sequence

of 117 frames. There would then be approximately 10,000 such events for a 30 second run, which is less than the number of pits observed during such a run in soft material by a factor of about 10. Thus, if the rebounding bubbles result from this uniquely damaging collapse, both the massive and smaller ones must be involved. However, the ratio between bubble collapses of all types near the surface and pits incurred by a soft aluminum specimen is about 7×10^3. Similarly enormous ratios were observed in our venturi tests and by other investigators for vibratory tests.[21] Hence, the ratio above for the particular type of collapse assumed to be damaging in this study is more realistic than previous observations in this respect.

CONCLUSIONS

Photographic proof was obtained of Noltingk and Neppiras's[4] theories that most bubbles in an ultrasonically induced cavitation field are expanded and collapsed in one acoustic cycle. Three models were hypothesized to explain the various types of bubbles found in the cavitation field and high-speed photographs were presented as partial substantiation of their existence.

It is believed that the "shock rings" greatly inhibit the population of transient bubbles in the vicinity of the overpressure.

If the normal collapse mode in ultrasonically-induced cavitation is toroidal, as this study appears to show, then those investigations which have assumed the symmetrical Rayleigh type collapse model incur an error both in collapse time and predicted pressure pulse from the collapse and rebound, since the toroidal collapse sequence is longer and has additional dissipative processes.

1 L. E. Robinson, B. A. Holmes, and W. C. Leith, "Progress Report on Standardization of the Vibratory Cavitation Test," Trans. Am. Soc. Mech. Engrs., pp. 103-107 (1958).

2 R. Garcia, "Comprehensive Cavitation Damage Data for Water and Various Liquid Metals Including Correlations with Materials and Fluid Properties," Ph.D. Thesis, University of Michigan (1966).

3 R. Garcia and F. G. Hammitt, "Cavitation Damage and Correlations with Materials and Fluid Properties," to be published Trans. Am. Soc. Mech. Engrs. J. Basic Engr. (1966).

4 B. E. Noltingk and E. A. Neppiras, "Cavitation Produced by Ultrasonics," Proc. Phy. Soc., (London) B63, pp. 674-685 (1950).

5 H. G. Flynn, "Physics of Acoustic Cavitation in Liquids," in Physical Acoustics, W. P. Mason, Ed. (Academic Press, New York, 1964), Vol. 1, Part B, Chap. 9, pp. 57-172.

6 G. W. Willard, "Ultrasonically Induced Cavitation in Water: A Step-by-Step Process," J. Acoust. Soc. Am. 25, pp. 669-686 (1953).

7 R. D. Ivany, F. G. Hammitt, and T. M. Mitchell, "Cavitation Bubble Collapse Observations in a Venturi," Trans. Am. Soc. Mech. Engrs. J. Basic Engr., 88, No. 3, pp. 649-651 (1966).

8 M. J. Robinson, "On the Detailed Flow Structure and the Corresponding Damage to Test Specimens in a Cavitating Venturi," Ph.D. Thesis, University of Michigan (1965).

9 M. J. Robinson and F. G. Hammitt, "Detailed Damage Characteristics in a Cavitating Venturi," to be published Trans. Am. Soc. Mech. Engrs., J. Basic Engr. (1967).

10 M. Kornfield and L. Survorov, "On the Destructive Action of Cavitation," J. Appl. Phys. 15, pp. 495-496 (1944).

11 C. F. Naude and A. T. Ellis, "On the Mechanism of Cavitation Damage by Hemispherical Cavities Collapsing in Contact with a Solid Boundary," Trans. Am. Soc. Mech. Engrs., J. Basic Engr., 83, No. 4, pp. 648-656 (1961).

12 Lord Rayleigh, "On the Pressure Developed in a Liquid During the Collapse of a Spherical Cavity," Phil. Mag. 34, pp. 94-98 (1917).

13 R. D. Ivany and F. G. Hammitt, "Cavitation Bubble Collapse in Viscous Compressible Liquids - Numerical Analyses," Trans. Am. Soc. Mech. Engrs., J. Basic Engrs., pp. 977-985 (1965).

14 R. Hickling and M. Plesset, "The Collapse and Rebound of a Spherical Cavity in Water," The Physics of Fluids, Vol. 7, No. 1, Jan. 1964, p. 7.

15 F. G. Hammitt, "Observations of Cavitations Damage in a Flowing System," J. Basic Eng., Trans. Am. Soc. Mech. Engrs. 85, pp. 347-359 (1963).

16 O. H. Engel, "Waterdrop Collisions with Solid Surfaces," J. of Research of National Bureau of Standards, 54 (1955).

17 J. Schmid, "Cinematographic Investigation of Single Bubble Cavitation," Acoustica 9, pp. 321-326 (1959).

18 A. T. Ellis, "Techniques for Pressure Pulse Measurement and High Speed Photography in Ultrasonic Cavitation," California Institute of Technology Report No. 21-20 (1955).

19 N. D. Shutler and R. B. Mesler, "A Photographic Study of the Dynamics and Damage Capabilities of Bubbles Collapsing Near Solid Boundaries," University of Kansas (1964).

20 F. B. Bowden, "The Formation of Micro Jets in Liquids Under the Influence of Impact or Shock," Phil. Trans. Royal Society A. No. 110, 260, pp. 94, 95 (1966).

21 M. S. Plesset, "Shock Waves from Cavitation Collapse," Phil. Trans. Royal Society A, No. 110, 260, pp. 241-244 (1966).

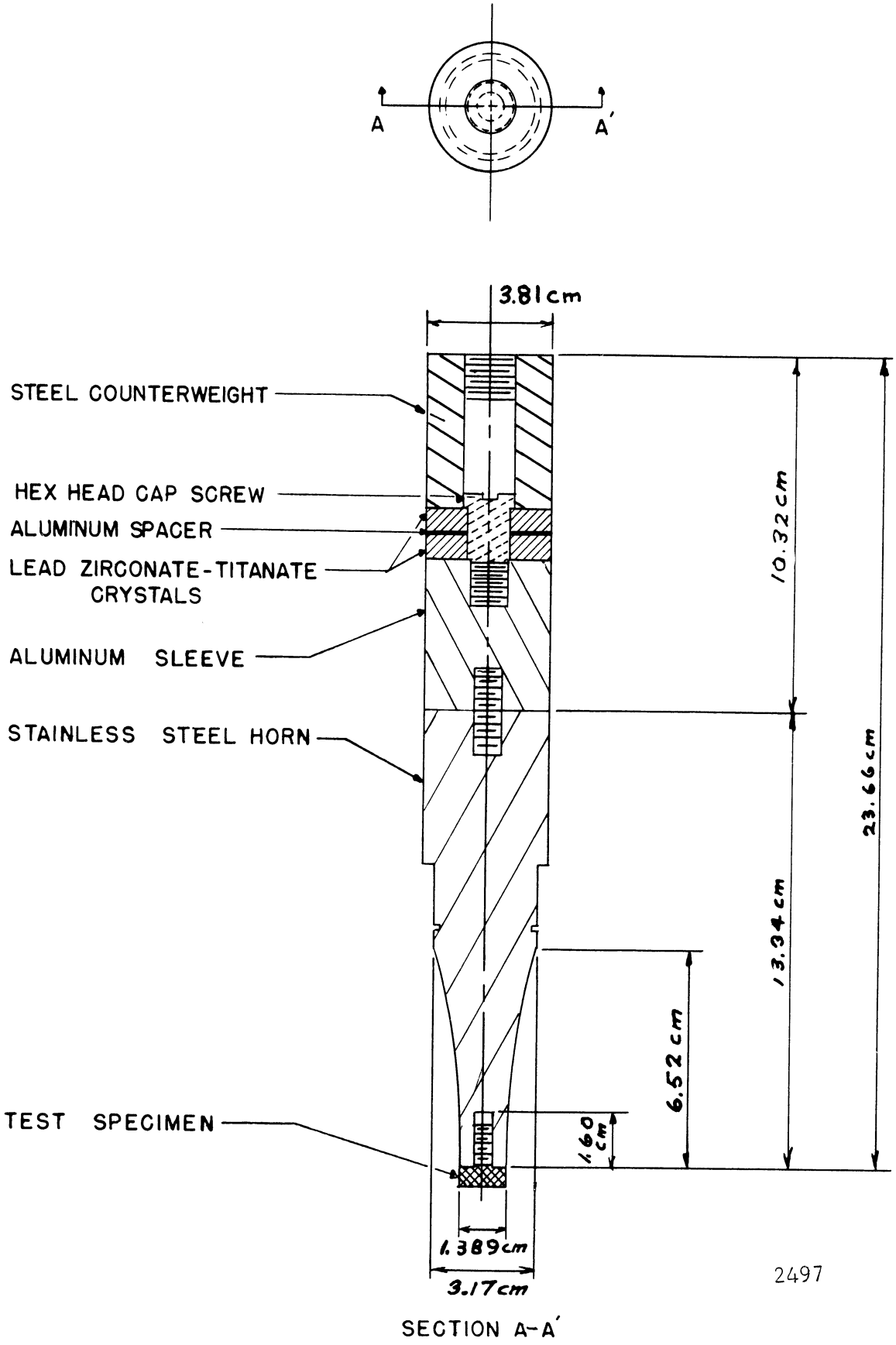

Fig. 1.--Exponential horn and ultrasonic transducer assembly showing test specimen mounted on lower end.

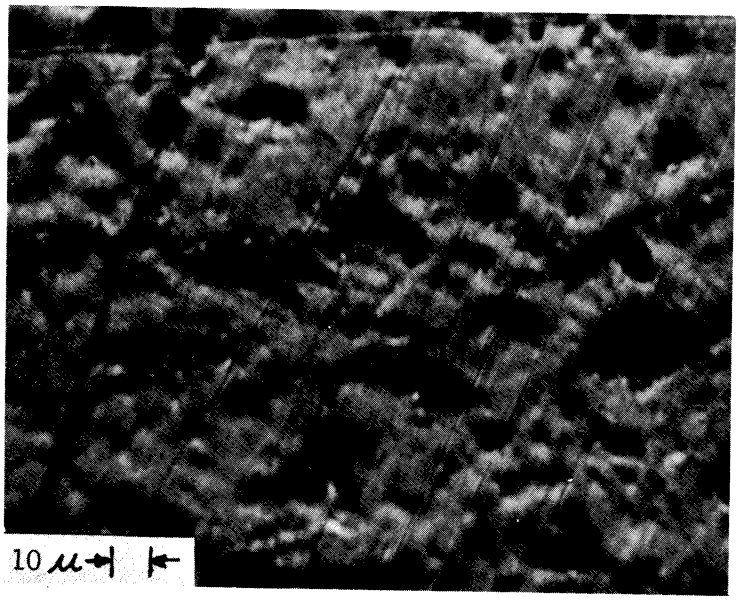

2498

Fig. 2.--Photomicrograph (500x) of a section from a type 6061-T651 aluminum specimen exposed to cavitation in water for 15 seconds.

Fig. 3.--High speed photographic sequence (a), (b) and (c) of a 1.389 cm diameter type 2024-T351 aluminum specimen showing the cavitation bubble field in water.

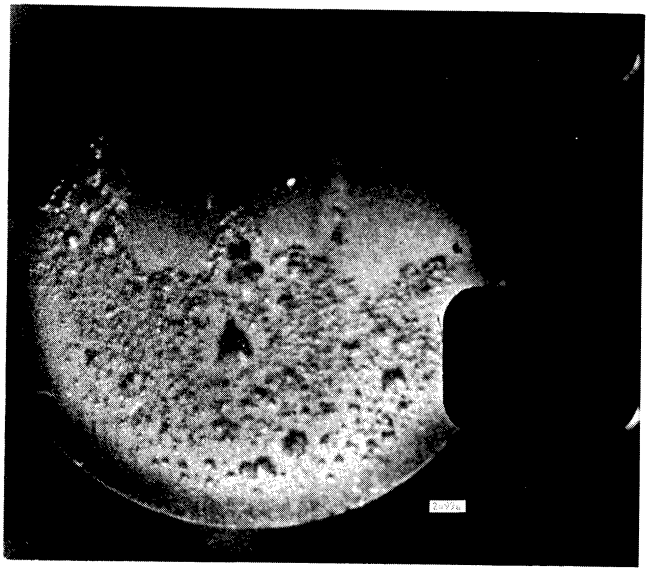

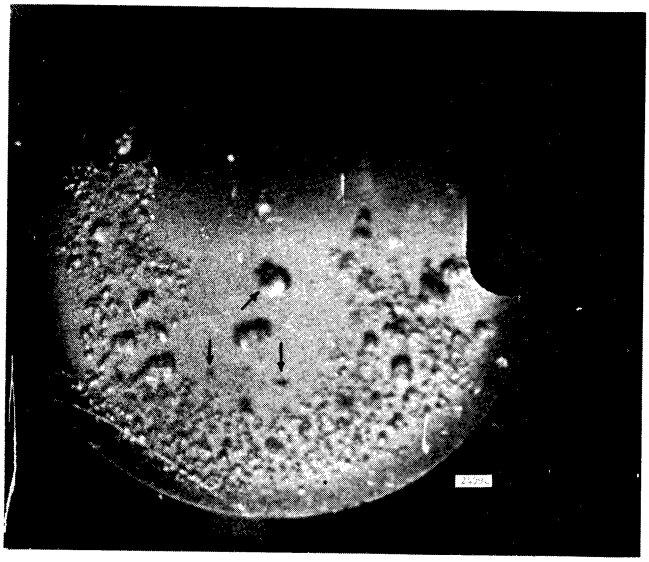

Fig. 4.--High speed photographic sequence (a), (b), (c), (d), (e), and (f) of a 1.389 cm diameter type 304 stainless steel specimen with upper half polished and lower half lightly abraded showing the cavitation bubble field in water.

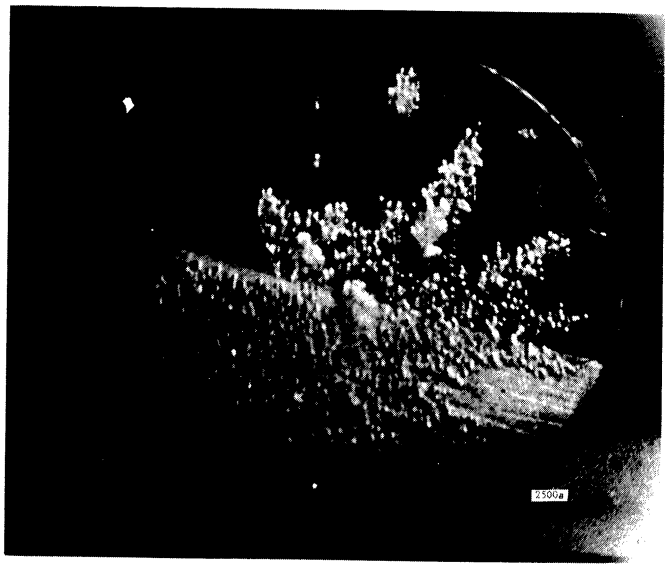
2500a

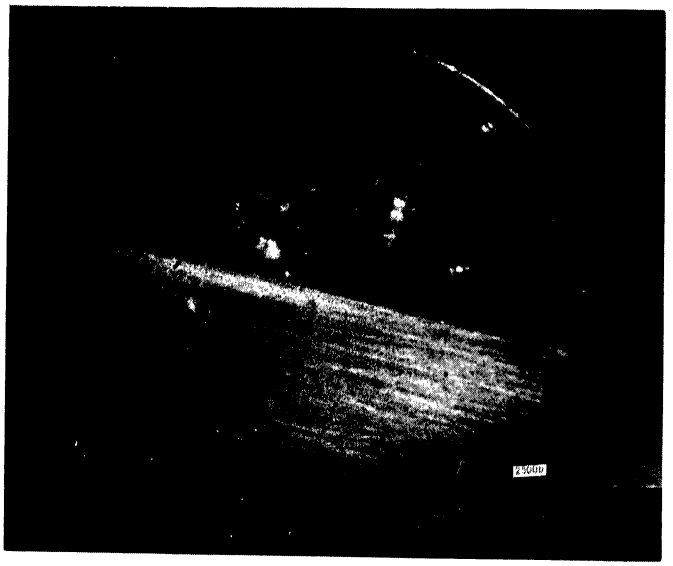
2500b

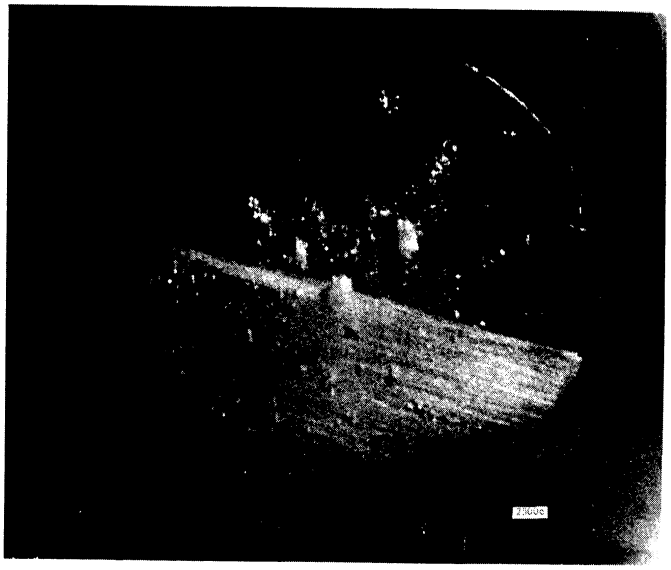
2500c

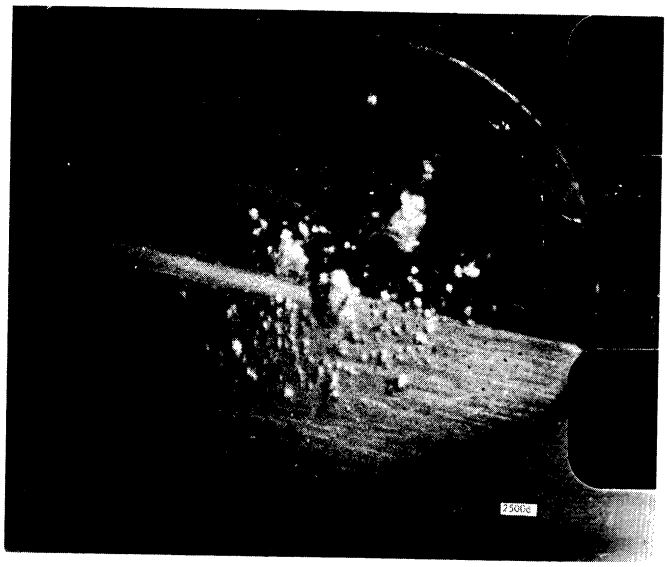
2500e

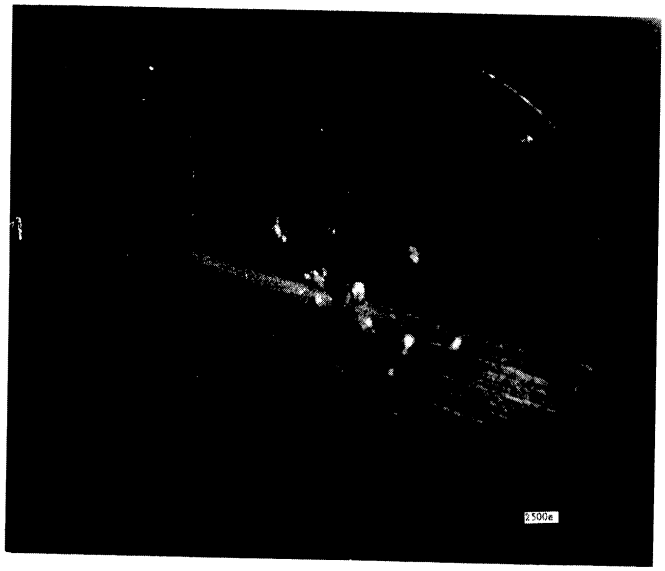
2500e

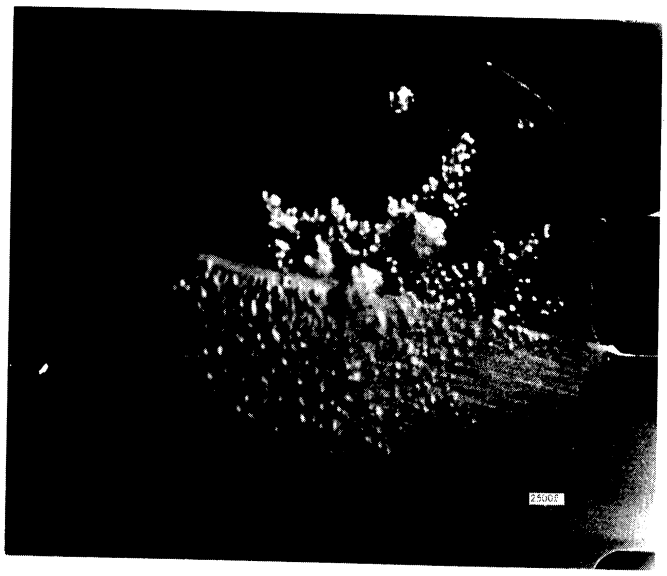
2500e

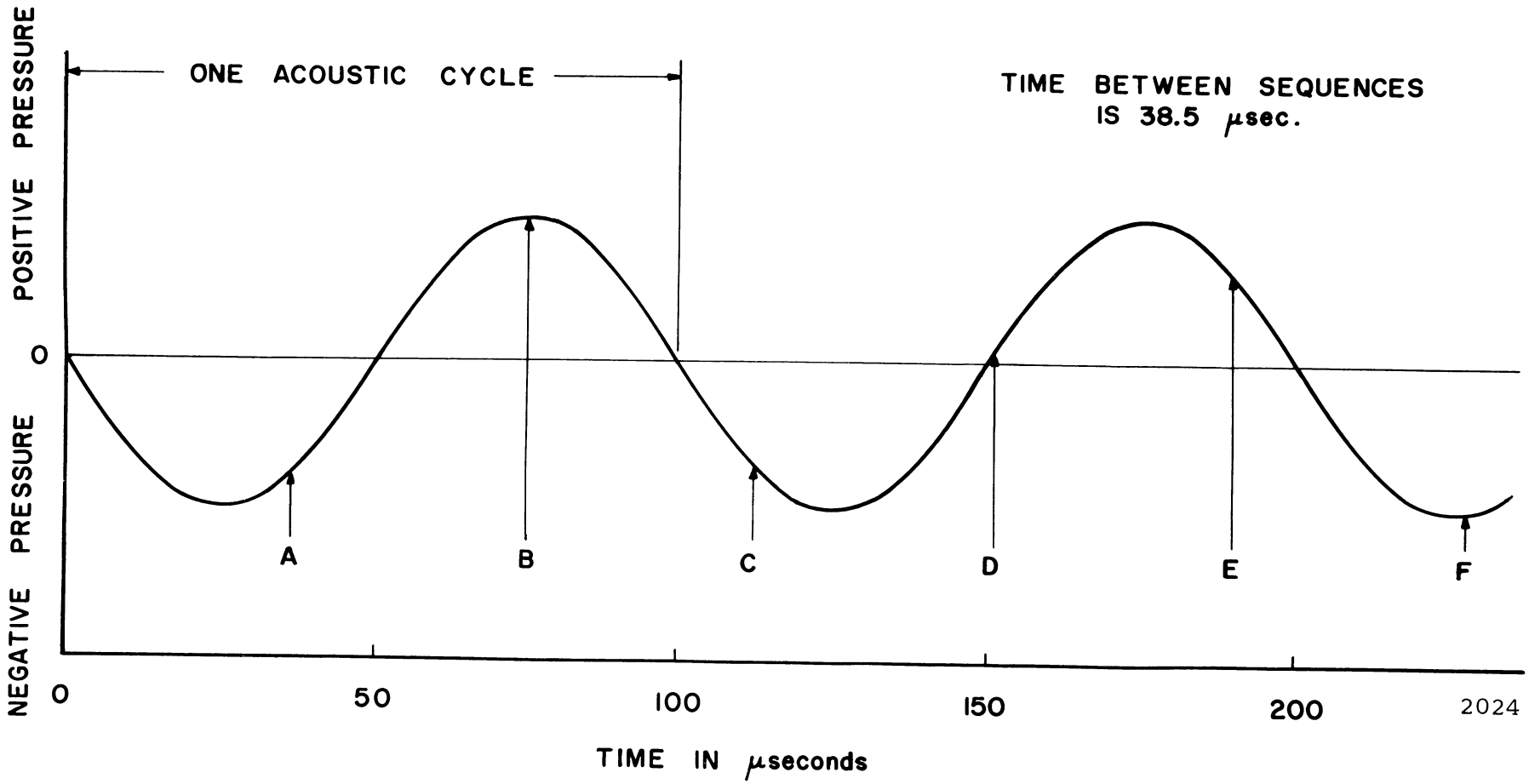

Fig. 5.--Predicted portions in the acoustic cycle of the high speed photographic sequence shown in Fig. 4.

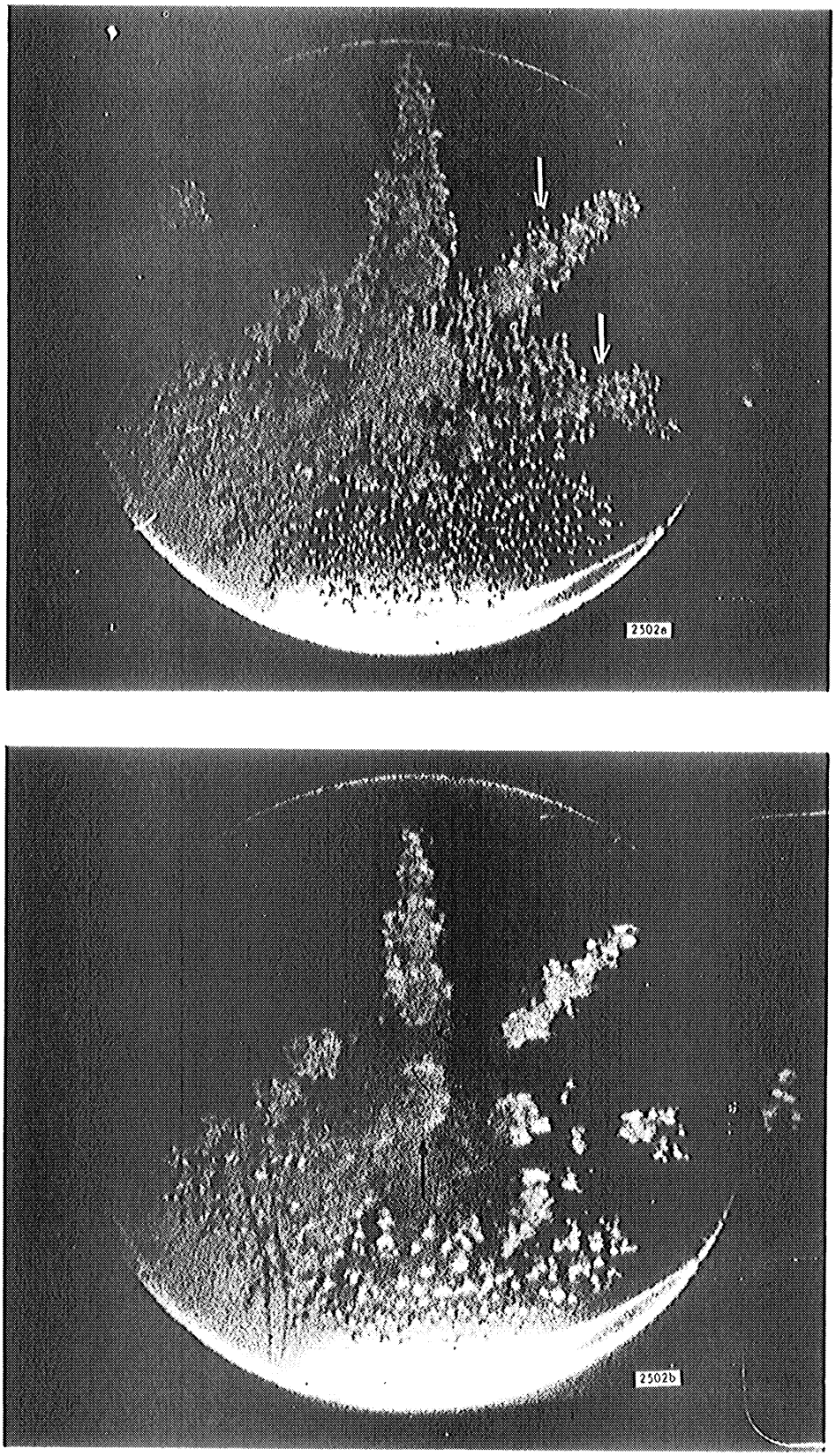

Fig. 6.--High speed photographs (a) and (b), not in sequence, of a 1.389 cm diameter type 304 stainless steel specimen with right half polished and left half lightly abraded showing the cavitation bubble field in water.

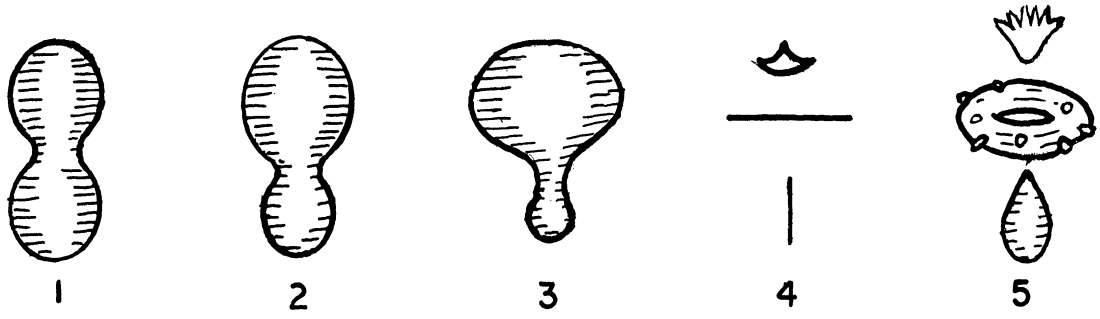

MODEL A

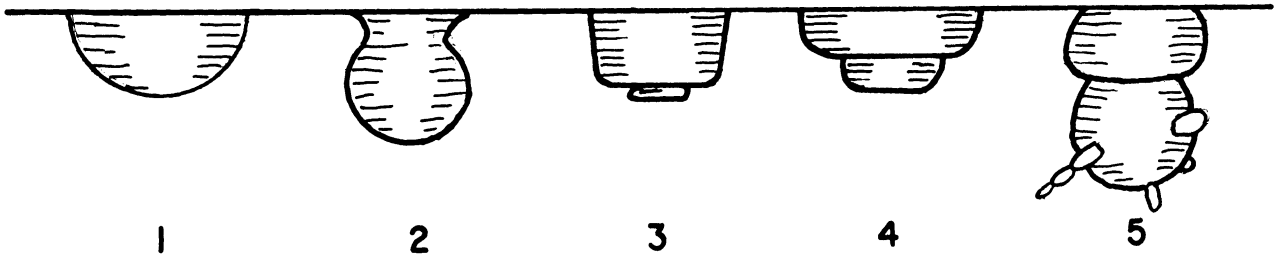

MODEL B

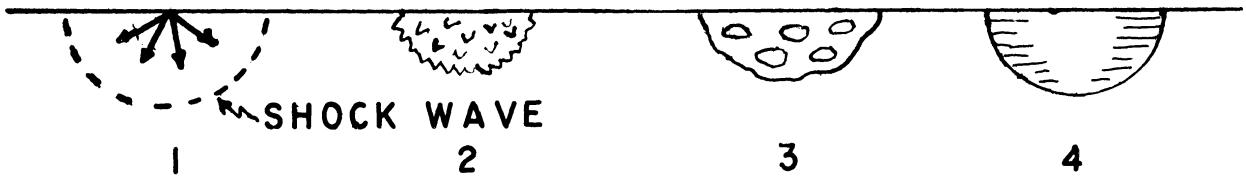

2503

MODEL C

Fig. 7.--A) Model for collapse and rebound of a spherically symmetrical bubble in a fluid on or adjacent to a surface; B) Model for partial collapse and rebound of hemispherically shaped bubble on a flat surface; C) Model for impact of a jet from a collapsing bubble on or adjacent to a surface and subsequent rebound to form a hemispherical bubble.

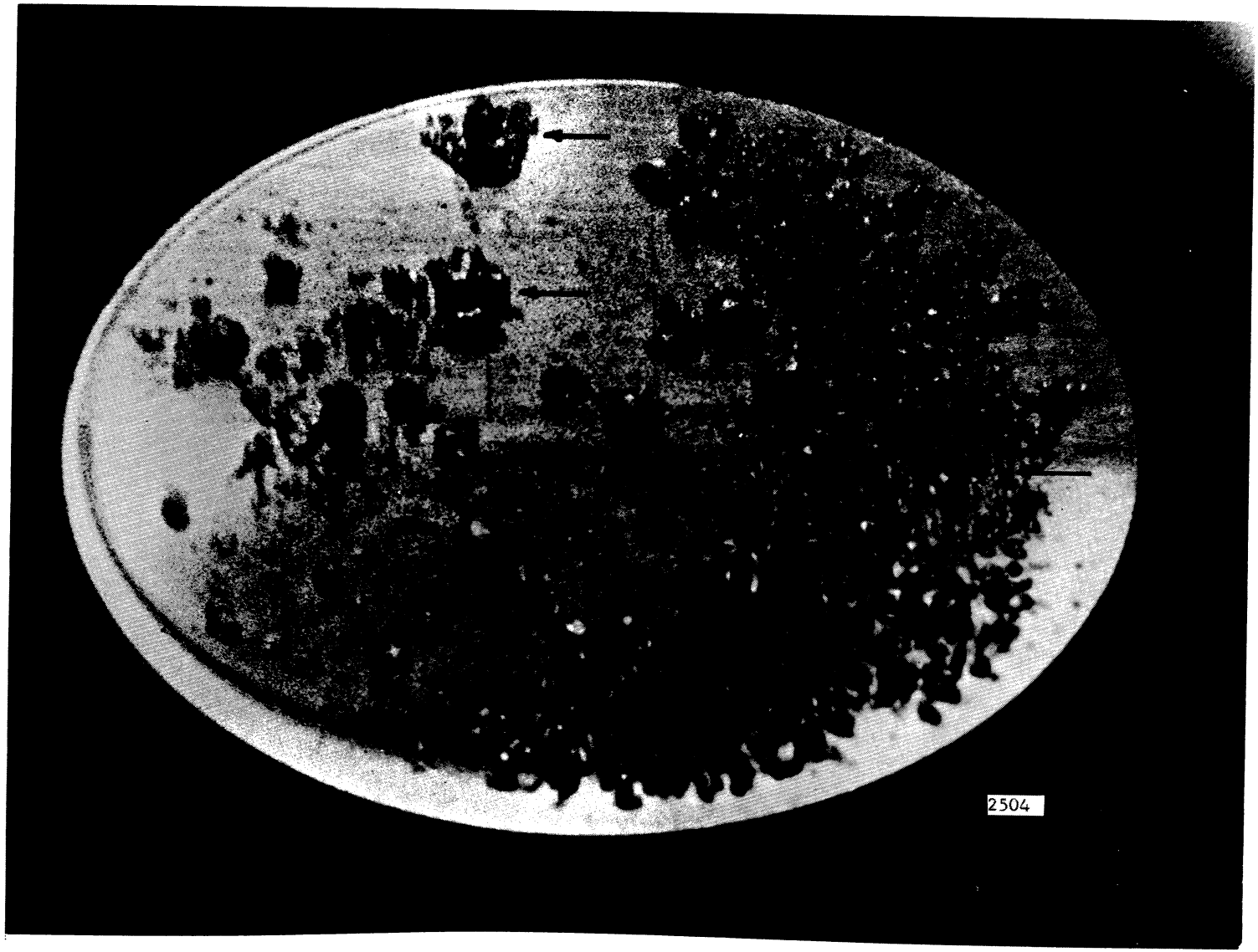

Fig. 8.--High speed photograph of a 1.389 cm diameter type 304 stainless steel specimen with upper half lightly abraded and lower half polished showing the cavitation bubble field in water.

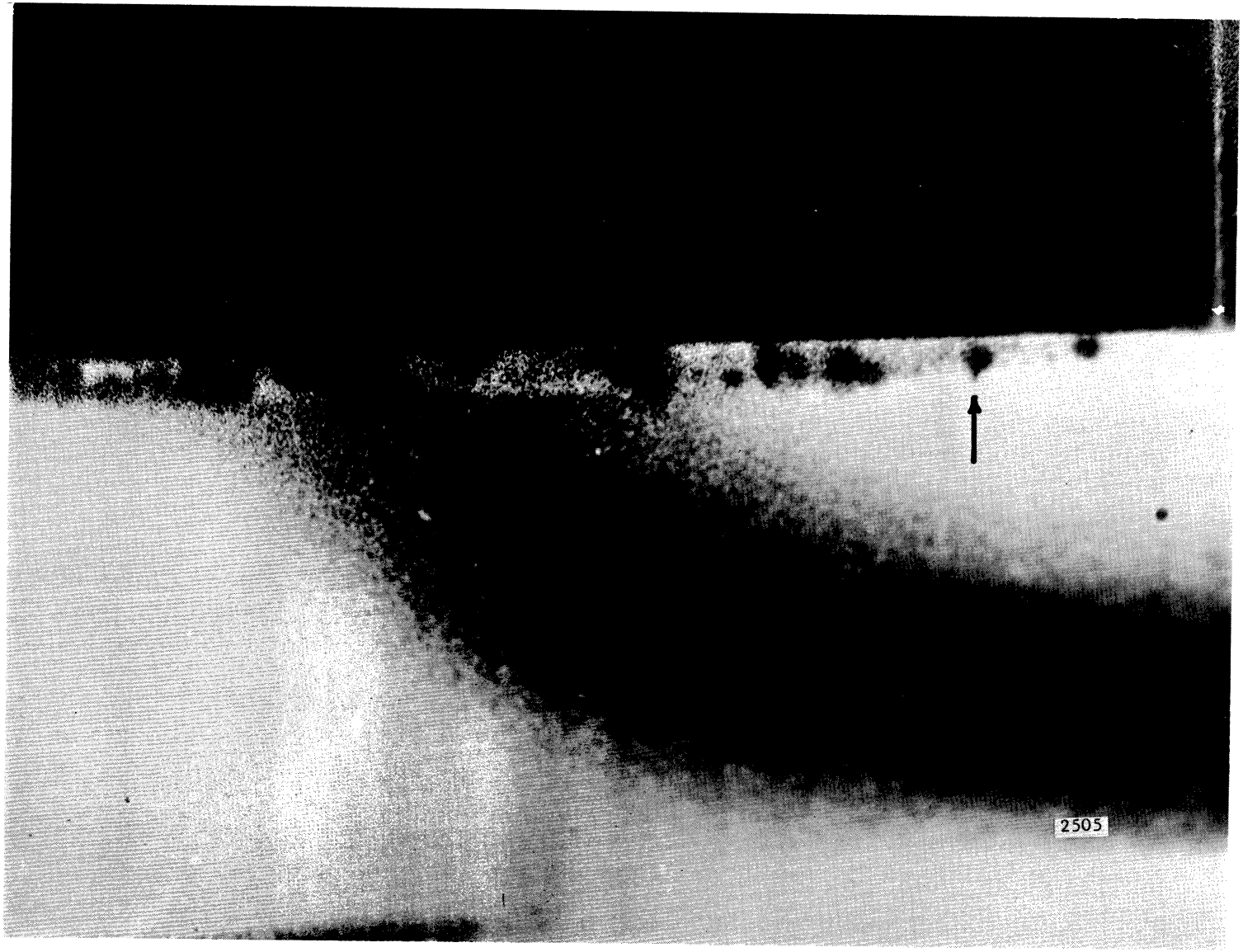

Fig. 9.--Arrow indicates a bubble of an approximate 0.25 mm diameter at the base believed to be in the collapse mode preceding the formation of a jet.

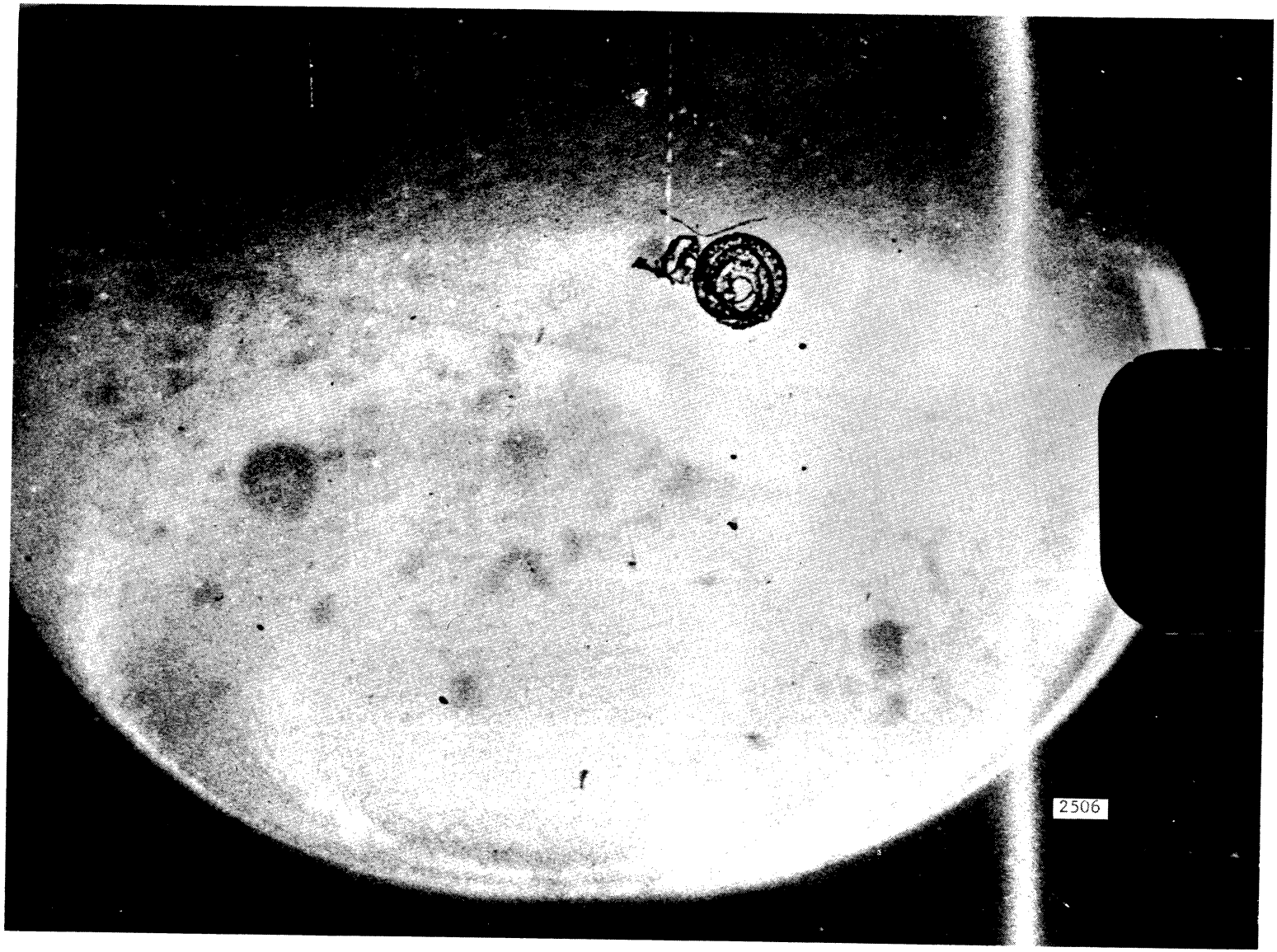

Fig. 10.--The result of the collapse and apparent rebound of large bubble in water at an approximate diameter at rebound of 1 mm.

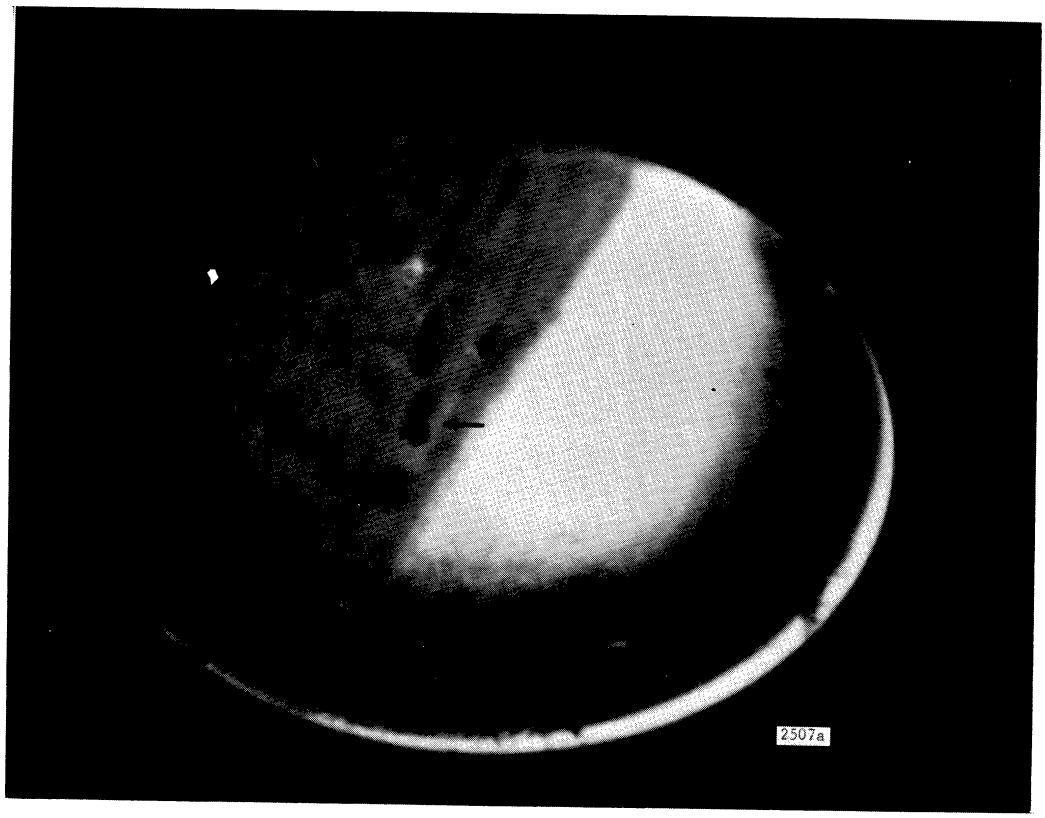

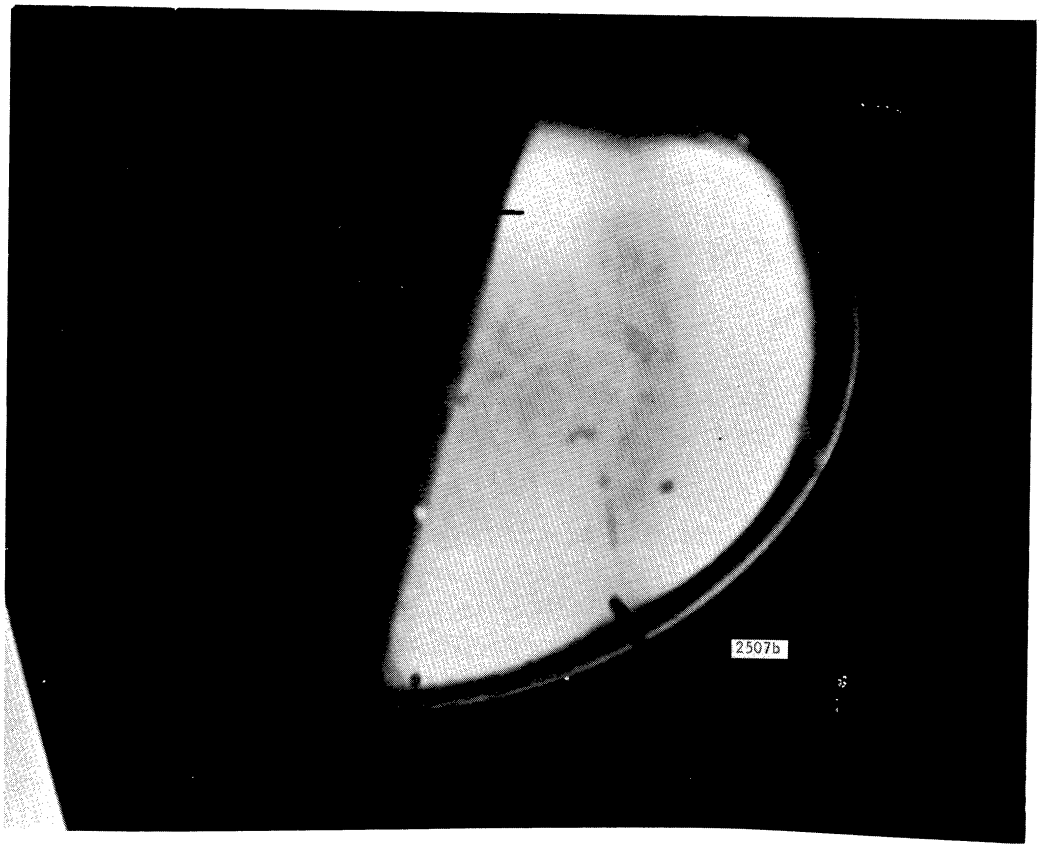

Fig. 11.--High speed photographs (a) and (b), not in sequence, of a 1.389 cm diameter type 304 stainless steel specimen with right half polished and left half lightly abraded showing the cavitation bubble field in water.

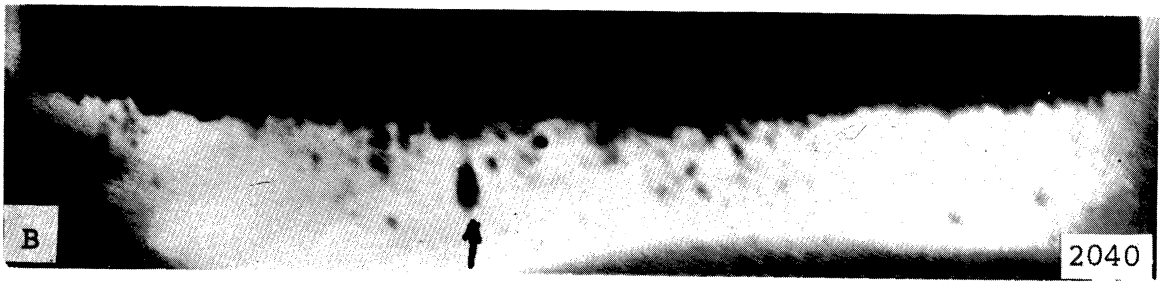

Fig. 12.--Pinched off section from a toroidal collapse approximately 0.27 mm in width is shown in a cavitation bubble field.

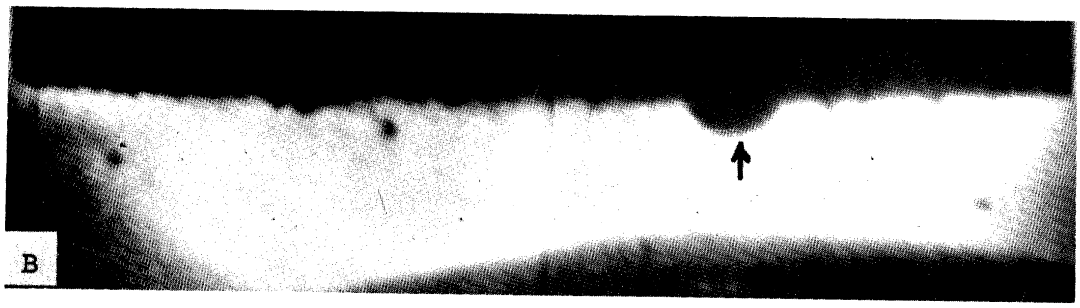

2509a

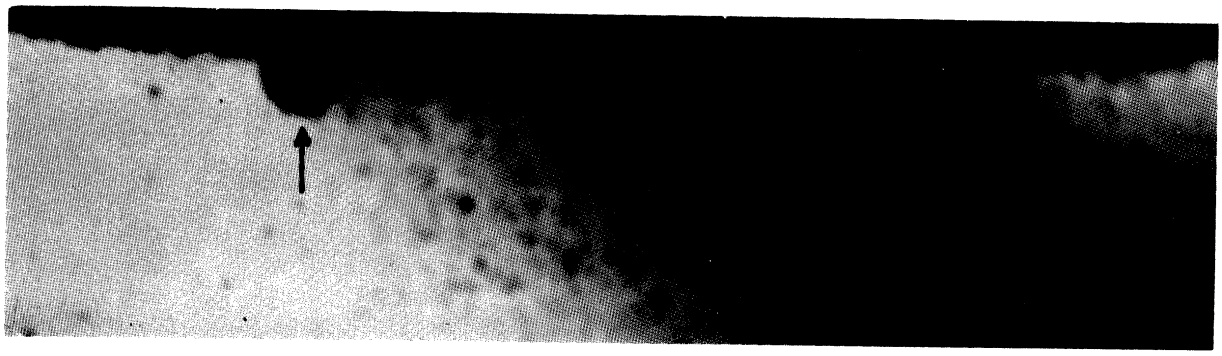

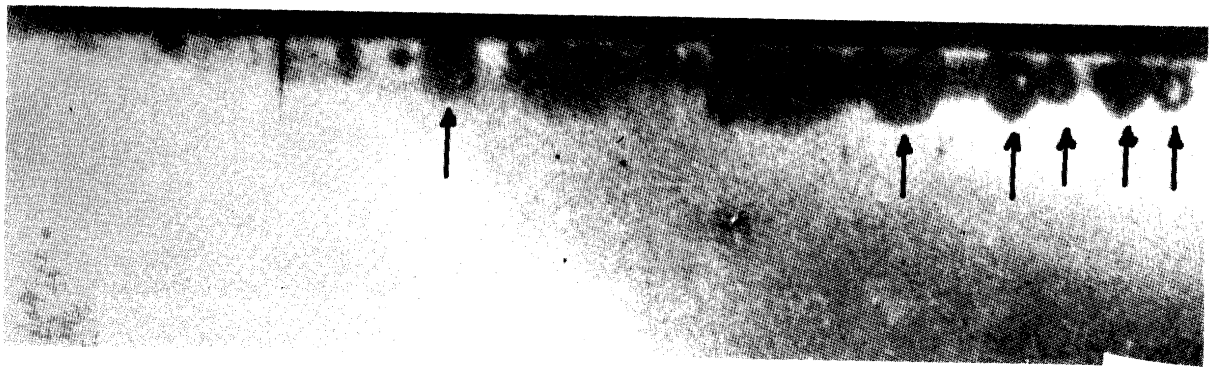

2509b

Fig. 13.--High speed photographs (a) and (b), not in sequence, showing a 1.20 mm diameter hemispherical bubble as in Model B-1 and shapes from 0.30 mm to 0.80 mm in diameter which are similar to Model B-2, respectively.

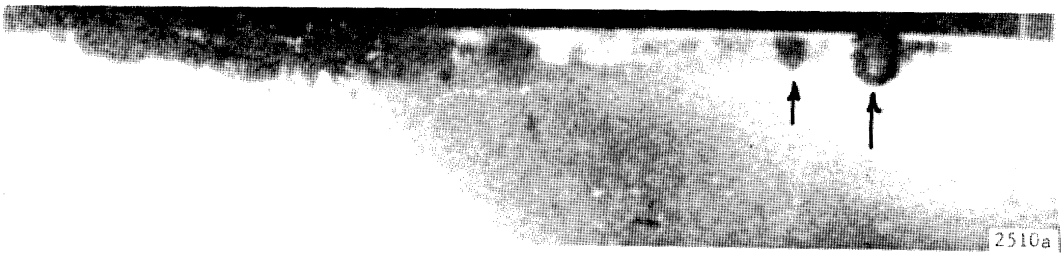

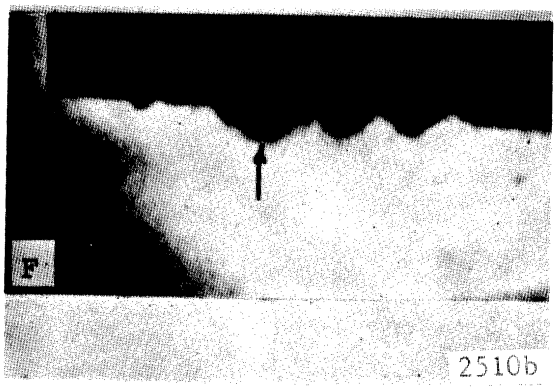

Fig. 14.--High speed photographs (a) and (b), not in sequence, showing bubbles 0.35 mm to 0.60 in diameter that are similar to Model B-3 and a bubble 1.40 mm in diameter similar to Model B-4.

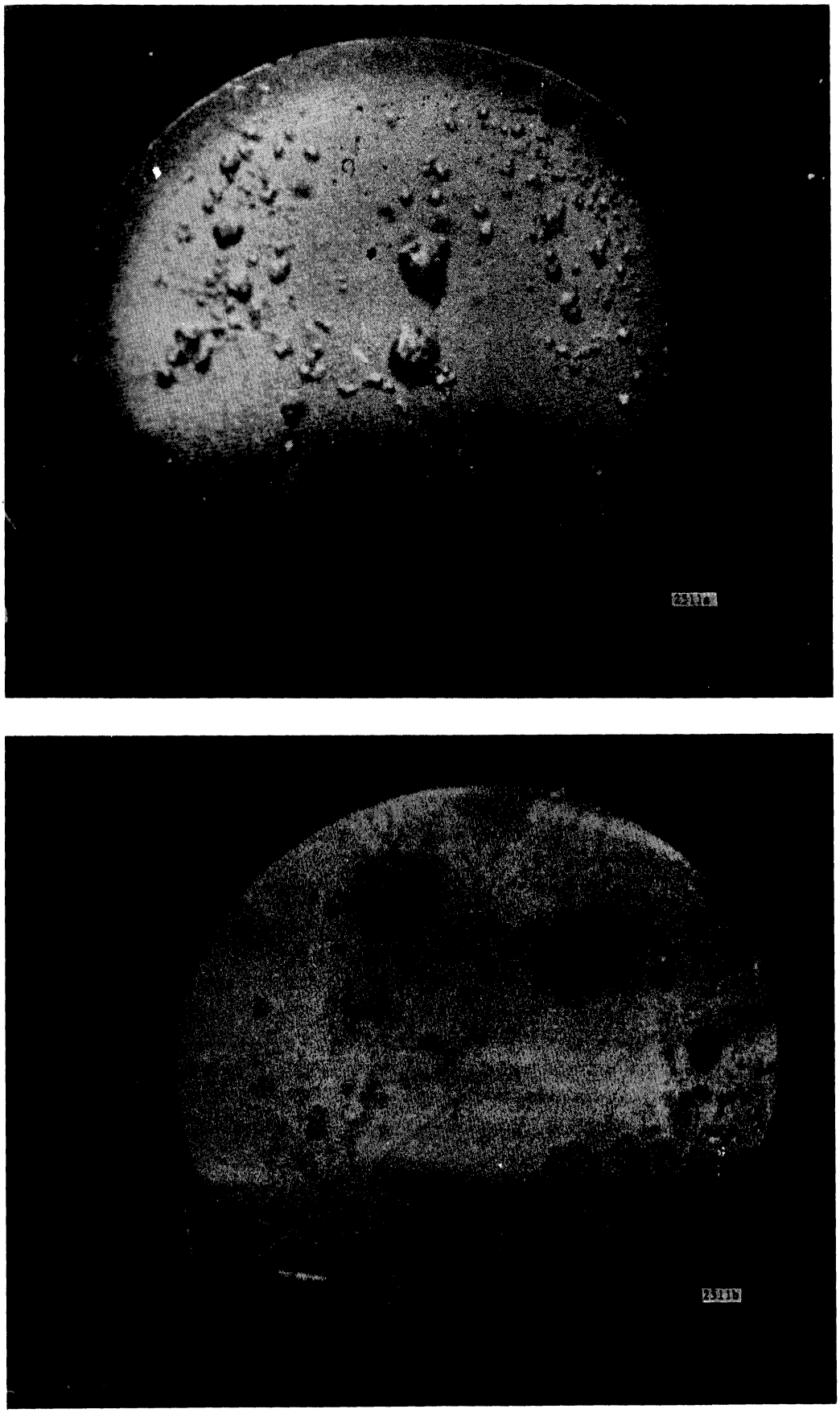

Fig. 15.--High speed photographs (a) and (b) of 1.389 cm diameter specimens showing cavitation bubble clouds in water with axis of the horn at an angle of 30^{o} from the horizontal.